

Radiative Corrections to High Energy Lepton Bremsstrahlung on Heavy Nuclei

Andrej B. Arbuzov

Joint Institute for Nuclear Research, 141980 Dubna, Russia

E-mail: `arbuzov@theor.jinr.ru`

Abstract

One-loop radiative corrections to the leptonic tensor in high energy bremsstrahlung on heavy nuclei are calculated. Virtual and real photon radiation is taken into account. Double bremsstrahlung is simulated by means of Monte Carlo. Numerical results are presented for the case of muon bremsstrahlung in conditions of the COMPASS experiment at CERN.

1 Introduction

Charged lepton Bremsstrahlung on nuclei has been studied both theoretically and experimentally for many years (see *e.g.* textbooks [1, 2] and references therein). This process contributes to energy losses of a lepton propagation through matter, which is relevant for many applications.

The similar process of high energy pion bremsstrahlung is used for extraction of pion polarizability [3, 4]. In the modern COMPASS experiment [5, 6] the muon bremsstrahlung is used as a reference cross section and for estimates of systematic uncertainties. For this reason differential distribution of the muon bremsstrahlung should be predicted with high accuracy. That requires to take into account several effects beyond the tree-level Born approximation. So one needs to consider multiple photon exchange with the nucleus (important for large Z values), electromagnetic nuclear elastic and inelastic form factors, screening of the nucleus by the electrons surrounding it, and inelastic interactions of the projectile particle with the atomic electrons (see Ref. [8] and references therein). Besides those, we have to take into account also the vacuum polarization in the exchanged photon and at least one-loop radiative corrections to the lepton tensor. In this paper a new calculation of the latter is presented.

Ref. [9] gives a comprehensive report on the calculation of one-loop corrections to virtual Compton scattering ($ep \rightarrow ep\gamma$). The lepton bremsstrahlung on a heavy nucleus we met here is a specific case of the general problem. Results of Ref. [9] for the Compton tensor also can't be directly applied to the problem under consideration, since the actual kinematical conditions (see Eq.(6) below) deserve a special treatment. The latter includes keeping an exact dependence on the lepton mass and providing numerical stability of the corresponding computer code.

Since for this kinematical region we have to keep the exact dependence on the lepton mass, analytic formulae for the corrections become lengthy and cumbersome. Moreover to provide a possibility to impose various experimental cuts, we perform integration over the final state phase space numerically.

The paper is organized as follows. In the next section we give the notation and the explicit expression for the Born cross section. Sect. 3 presents the calculation of various radiative correction contributions: the one due to a single virtual loop, the one due to additional soft photon emission, and the one due to double bremsstrahlung. Numerical results and conclusions are given in the last section.

2 Preliminaries

At the Born level we can represent the differential spectrum of the hard photon produced in the process

$$l(p_1) + A(P) \rightarrow l(p_2) + \gamma(k) + A(P') \quad (1)$$

in the form [1, 2]

$$\begin{aligned} \frac{d\sigma^{\text{Born}}}{d\omega} = & \frac{Z^2\alpha^3}{2\pi} \int_{-1}^1 dc_1 \int_{-1}^1 dc_2 \int_0^{2\pi} d\varphi \frac{|\mathbf{p}_2|}{|\mathbf{p}_1|} \frac{\omega}{Q^4} \left(\frac{|\mathbf{p}_2|^2}{\chi_2^2} (4E_1^2 - Q^2) s_2^2 + \frac{|\mathbf{p}_1|^2}{\chi_1^2} (4E_2^2 - Q^2) s_1^2 \right. \\ & \left. + 2 \frac{\omega^2}{\chi_1 \chi_2} (|\mathbf{p}_1|^2 s_1^2 + |\mathbf{p}_2|^2 s_2^2) - 2 \frac{|\mathbf{p}_1||\mathbf{p}_2|}{\chi_1 \chi_2} (2E_1^2 + 2E_2^2 - Q^2) s_1 s_2 \cos \varphi \right), \end{aligned} \quad (2)$$

where $\omega = k^0$ is the emitted photon energy; φ is the azimuthal angle of the scattered lepton; Z is the nucleus charge; m is the lepton mass; $E_{1(2)}$ and $p_{1(2)}$ are the energies and 4-momenta of the projectile (scattered) leptons,

$$c_{1,2} = \cos(\widehat{\mathbf{k}\mathbf{p}_{1,2}}), \quad s_{1,2} = \sin(\widehat{\mathbf{k}\mathbf{p}_{1,2}}), \quad \chi_{1,2} = kp_{1,2}, \quad Q^2 = -(p_1 - p_2 - k)^2. \quad (3)$$

Here and in what follows, it is assumed that the lepton mass is small compared with the atom mass, while the energies are large:

$$m \ll M_A, \quad E_1 \gg m, \quad E_2 \gg m, \quad \omega \gg m. \quad (4)$$

Let us rewrite the Born cross section (2) via a set of form factors:

$$\begin{aligned} \frac{d\sigma^{\text{Born}}}{d\omega} = & \frac{Z^2\alpha^3}{2\pi} \int_{-1}^1 dc_1 \int_{-1}^1 dc_2 \int_0^{2\pi} d\varphi \frac{|\mathbf{p}_2|}{|\mathbf{p}_1|} \frac{\omega}{Q^4} \frac{1}{2e^4} \left(\mathcal{F}_\delta^{(0)}(q_s, t_s, u_s) - \mathcal{F}_{11}^{(0)}(q_s, t_s, u_s) E_2^2 \right. \\ & \left. - \mathcal{F}_{22}^{(0)}(q_s, t_s, u_s) E_1^2 + \mathcal{F}_{12}^{(0)}(q_s, t_s, u_s) E_2 E_1 + \mathcal{F}_{21}^{(0)}(q_s, t_s, u_s) E_1 E_2 \right), \end{aligned} \quad (5)$$

$$q_s = 2\chi_2 - 2\chi_1 + Q^2, \quad t_s = 2\chi_1 - m^2, \quad u_s = -2\chi_2 - m^2,$$

where e is the electron charge. The notation in the above expression is adjusted to the one used in the SANC [11] system, where the relevant expressions can be found as for the Born-level form factors as well as for the ones in the one-loop approximation.

Studying the differential distribution in the scattering angles of the Born cross section, one can see that it is peaked in the kinematical domain, where

$$\widehat{k\mathbf{p}}_{1,2} \sim \widehat{\mathbf{p}_1\mathbf{p}_2} \sim \frac{m}{E_1}. \quad (6)$$

For the case of high energy muon scattering ($E_1 \sim 100$ GeV) being under consideration now, the angles become small. Moreover, one should be careful with the dependence on the lepton mass, since $m^2 \sim \chi_{1,2}$ in this domain. On the other hand, we can safely drop some terms, proportional to the small ratio m^2/E_1^2 . As concerning the momentum transferred, contrary to the case of the Rutherford scattering, it can't go down below the kinematical threshold value

$$Q_{\min} \equiv \sqrt{Q_{\min}^2} = \frac{m^2 \omega}{2E_1 E_2}. \quad (7)$$

In the ultra-relativistic approximation applicable in our case, after an integration over the whole phase space, one gets the Born-level photon spectrum in the simple form

$$\frac{d\sigma}{d\omega} = \frac{4Z^2\alpha^3}{m_\mu^2\omega E_1^2} \left(E_1^2 + E_2^2 - \frac{2}{3}E_1 E_2 \right), \quad \omega = E_1 - E_2. \quad (8)$$

3 One-Loop Corrections

We subdivide the contributions of the one-loop QED corrections into three parts: 1) the one due to a single virtual loop; 2) the one due to soft real photon emission; 3) and the one due to additional hard photon emission (double bremsstrahlung).

3.1 Virtual Loop Contribution

Representatives of the Feynman diagrams corresponding to the first type of corrections are shown in Fig. 3.1. This contribution was computed with help of the automatized computer system SANC [11]. The system provided the set of form factors calculated keeping the exact dependence on the lepton mass. The form factors are expressed via a number of one-loop master integrals (Passarino–Veltman functions), which are called from a SANC library. The infrared divergence in the relevant integrals is regularized by a fictitious photon mass λ . So, the virtual loop contribution takes the form

$$\begin{aligned} \frac{d\sigma^{\text{Virt}}}{d\omega} = & \frac{Z^2\alpha^3}{2\pi} \int_{-1}^1 dc_1 \int_{-1}^1 dc_2 \int_0^{2\pi} d\varphi \frac{|\mathbf{p}_2|}{|\mathbf{p}_1|} \frac{\omega}{Q^4} \frac{1}{16\pi^2 e^4} \left(\mathcal{F}_\delta^{(1)}(q_s, t_s, u_s) - \mathcal{F}_{11}^{(1)}(q_s, t_s, u_s) E_2^2 \right. \\ & \left. - \mathcal{F}_{22}^{(1)}(q_s, t_s, u_s) E_1^2 + \mathcal{F}_{12}^{(1)}(q_s, t_s, u_s) E_2 E_1 + \mathcal{F}_{21}^{(1)}(q_s, t_s, u_s) E_1 E_2 \right). \end{aligned} \quad (9)$$

Here we adopt the SANC notation for the arguments and the normalization of the form factors. More details about the evaluation of form factors for such processes within SANC can be found in Ref. [12].

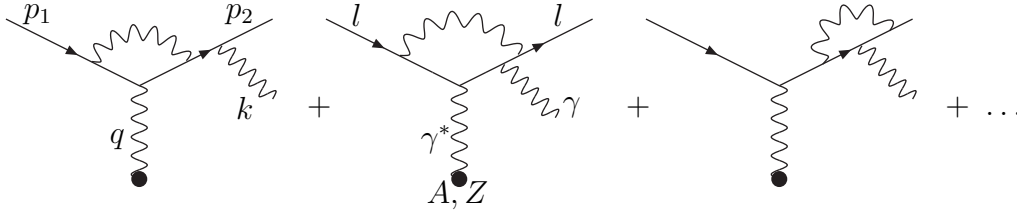


Figure 1: Representatives of Feynman amplitudes with single virtual loops.

3.2 Soft Photon Contribution

Using the phase space slicing method we define the soft photon contribution as the one of the process with emission of an additional photon with energy below a certain value $\bar{\omega}$, which is small compared with the beam energy. In our calculations we perform the spicing in the laboratory reference frame where the nucleus is at rest. Using the standard techniques of soft photon emission calculations we get the corresponding correction, which is factorized before the Born cross section:

$$\begin{aligned}
\frac{d\sigma^{\text{Soft}}}{d\omega} &= \delta^{\text{Soft}} \frac{d\sigma^{\text{Born}}}{d\omega}, \quad \delta^{\text{Soft}} = -\frac{\alpha}{4\pi^2} \left(I_{11} + I_{12} - 2I_{12} \right), \\
I_{11} &= 4\pi \left[\ln \frac{2\bar{\omega}}{\lambda} + \frac{1}{2\beta_1} \ln \left(\frac{1-\beta_1}{1+\beta_1} \right) \right], \quad I_{22} = 4\pi \left[\ln \frac{2\bar{\omega}}{\lambda} + \frac{1}{2\beta_2} \ln \left(\frac{1-\beta_2}{1+\beta_2} \right) \right], \\
I_{12} &= \frac{2\pi}{1-m^2/(a_{12}p_1p_2)} \left[2 \ln \frac{2\bar{\omega}}{\lambda} \ln a_{12} + \frac{1}{4} \ln^2 \left(\frac{1-\beta_1}{1+\beta_1} \right) - \frac{1}{4} \ln^2 \left(\frac{1-\beta_2}{1+\beta_2} \right) \right. \\
&\quad + \text{Li}_2 \left(1 - \frac{a_{12}E_1}{v_{12}}(1+\beta_1) \right) - \text{Li}_2 \left(1 - \frac{E_2}{v_{12}}(1+\beta_2) \right) \\
&\quad \left. + \text{Li}_2 \left(1 - \frac{a_{12}E_1}{v_{12}}(1-\beta_1) \right) - \text{Li}_2 \left(1 - \frac{E_2}{v_{12}}(1-\beta_2) \right) \right], \\
\beta_{1,2} &= \frac{|\mathbf{p}_{1,2}|}{E_{1,2}} = \sqrt{1 - \frac{m^2}{E_{1,2}^2}}, \quad a_{12} = \frac{p_1p_2}{m^2} \left(1 + \sqrt{1 - \frac{m^4}{(p_1p_2)^2}} \right), \\
v_{12} &= \frac{a_{12}p_1p_2 - m^2}{a_{12}E_1 - E_2}, \quad p_1p_2 = \frac{1}{2}Q^2 + \chi_2 - \chi_1 + m^2.
\end{aligned} \tag{10}$$

The infrared divergence of the soft photon contribution is regularized by means of a fictitious photon mass λ , the same as in the virtual loop contribution. One of the internal cross checks of the calculation is the cancellation of the dependence on this auxiliary parameter in the the sum of two contributions.

3.3 Double Bremsstrahlung Contribution

Here we start with the completely differential expression for the matrix element squared. Some of the Feynman diagrams for this process are shown in Fig. 3.3. The two photons are treated in a symmetric way. In particular, the condition $\omega_{1,2} > \bar{\omega}$ is applied for both the photons. The identity factor $1/2!$ is taken into account. Cancellation of the dependence on the parameter $\bar{\omega}$ is checked numerically in the sum of the soft and hard contributions. The contributions of double real photon emission is computed by means a Monte Carlo integrator

based on the VEGAS algorithm [13]. Seven-fold integration over the whole final state phase space (including integration of the detected photon energy) is performed. The distribution in the detected photon energy is extracted in course of the integration using weights provided by VEGAS for each thrown kinematical point.

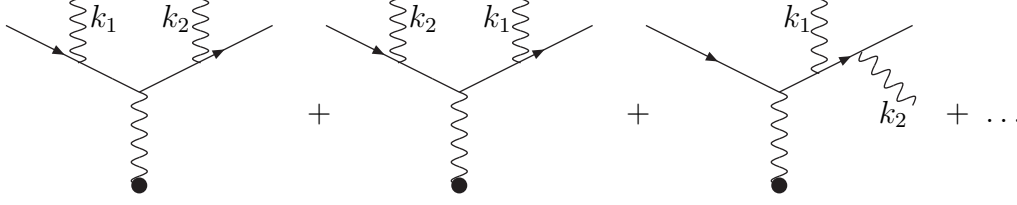


Figure 2: Representatives of Feynman amplitudes for double bremsstrahlung.

4 Numerical Results and Conclusions

Summing up the considered above contributions we get the 1-loop corrected cross section in the form

$$\frac{d\sigma^{\text{Corr}}}{d\omega} = \frac{d\sigma^{\text{Born}}}{d\omega} + \frac{d\sigma^{\text{Virt}}}{d\omega} + \frac{d\sigma^{\text{Soft}}}{d\omega} + \frac{d\sigma^{\text{Hard}}}{d\omega}. \quad (11)$$

In Table 4 there are numerical results for the specific contributions obtained for the following set of conditions:

$$\begin{aligned} E_1 &= 190 \text{ GeV}, & Z &= 82, & Q_{\text{max}}^2 &= 0.0075 \text{ GeV}^2, \\ \bar{\omega} &= 0.001 \text{ GeV}, & M_{\text{max}} &= 3.75 \cdot m_\mu, & P_{\text{min}}^\perp &= 0.045 \text{ GeV}, \\ m_l &= m_\mu = 0.10566 \text{ GeV}, \end{aligned} \quad (12)$$

where M_{max} is the maximal allowed invariant mass of the muon plus hard photon final state system; P_{min}^\perp is the minimal allowed transverse momentum of the outgoing muon; Z is the Pb nucleus charge. For the sake of simplicity, while computing the numbers for the Table we put a simple cut on the second hard photon energy: $\omega_2 < \omega_1$. By subscripts 1 and 2 we denote the results obtained with $\bar{\omega} = 10^{-3}$ and $\bar{\omega} = 10^{-4}$, respectively. The relative corrections $\delta_{1,2}$ are computed as

$$\delta_{1,2} = \frac{d\sigma^{\text{Virt}}/d\omega + d\sigma_{1,2}^{\text{Soft}}/d\omega + d\sigma_{1,2}^{\text{Hard}}/d\omega}{d\sigma^{\text{Born}}/d\omega} \cdot 100\%. \quad (13)$$

For a realistic simulation of spacial resolution and cluster energy threshold of the COMPASS calorimeter in addition to the conditions (12), we apply the following treatment of events with two hard photons:

- 1) $\max(\omega_1, \omega_2) \geq \omega_{\text{th}}$, *i.e.* at least one of the photons should have an energy exceeding the threshold;
- 2) if both the photons have energies above the threshold and the angle between their momenta is more than $\theta_{\gamma\gamma}$, the event is dropped;

ω/E_1	Born	Virtual	Soft ₁	Hard ₁	δ_1 , %	Soft ₂	Hard ₂	δ_2 , %
0.3	15677(1)	76.8(4)	- 260.1(1)	226.9(3)	+0.28	-307.0(1)	273.7(3)	+0.28
0.5	10836(1)	77.9(2)	- 319.0(1)	280.0(3)	+0.36	-377.4(1)	338.1(3)	+0.36
0.7	7337.7(1)	76.9(2)	- 363.3(1)	297.1(2)	+0.15	-430.9(1)	364.8(2)	+0.15
0.9	1267.4(1)	20.5(1)	- 111.1(2)	65.9(1)	-1.95	-132.4(2)	87.2(1)	-1.95

Table 1: Contributions to the corrected differential cross section in pbarn/GeV *versus* the photon energy fraction.

- 3) if the angle between their momenta is less than $\theta_{\gamma\gamma}$, the reconstructed photon energy is taken as the sum of the two: $\omega = \omega_1 + \omega_2$;
- 4) if one of the photon energies is below the threshold, the reconstructed photon energy is taken as the sum of the two: $\omega = \omega_1 + \omega_2$.

The parameter values correspond to one of data analysis procedures used by the COMPASS experiment,

$$\omega_{\text{th}} = 7 \text{ GeV}, \quad \theta_{\gamma\gamma} = 3 \text{ mrad}. \quad (14)$$

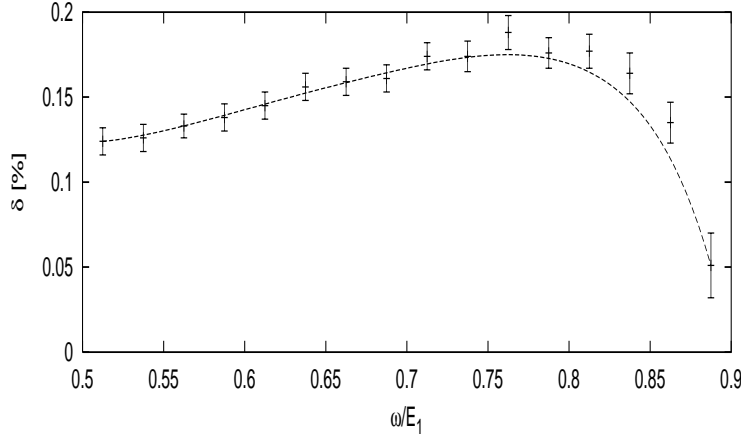


Figure 3: Relative contribution of one-loop corrections for realistic set-up *vs.* the photon energy fraction.

For the realistic set-up, the size of the resulting correction is found to be below the one percent level. That is due to the fact that the correction is proportional to $\alpha/(2\pi)$, and in our case there is no any enhancement factors. In particular, even so that the beam energy is so large compared with the muon mass, the contributions of the order $\mathcal{O}(\alpha \ln(E_1^2/m_\mu^2))$ cancel out in the sum of different contributions due to destructive interference of the initial and final state radiation. As can be seen from the Table 4 at the end of the spectrum ($\omega \rightarrow E_1$), where the phase space of additional hard photon emission is vanishing, we have a negative peak of the resulting radiation correction, which behaves there like $\alpha \ln((E_1 - \omega)/E_1)$. But this peak is effectively washed out from the end of the spectrum in Fig. 4, because of the the additional conditions (14) on event selections.

An analogous study was performed for the case of pion bremsstrahlung in Ref. [14], where a similar behavior and magnitude of the one-loop corrections have been obtained within the scalar QED.

Acknowledgments

I am grateful to the SANC team for providing codes for the form factors. I would like to thank B. Bardin, S. Bondarenko, A. Guskov, L. Kalinovskaya, Z. Kroumchtein, and A. Olshevsky for fruitful discussions. This work was supported by the INTAS grant 03-51-4007 and by the RFBR grant 07-02-00932.

References

- [1] A.I. Akhiezer, V.B. Berestecki, *Quantum Electrodynamics*, New. York, Wiley Interscience, 1969.
- [2] V.B. Berestetskii, E.M. Lifshitz, and L.P. Pitaevskii, *Quantum Electrodynamics*, 2nd ed., Oxford, Pergamon Press, 1982.
- [3] Yu.M. Antipov *et al.*, Phys. Lett. B **121** (1983) 445.
- [4] M. Moinester, *Pion polarizabilities and hybrid meson structure at CERN COMPASS*, arXiv:hep-ex/0012063.
- [5] P. Abbon *et al.* [COMPASS Collaboration], Nucl. Instrum. Meth. A **577** (2007) 455.
- [6] COMPASS Collaboration, G. Baum *et al.*, *COMPASS: A proposal for a COmmon Muon and Proton Apparatus for Structure and Spectroscopy*, CERN/SPSLC 96-14, SPSC/P 297 (March 1996).
- [7] F. Bradamante, G. Mallot, S. Paul (Eds.), *Workshop on future physics at COMPASS*, CERN, Geneva, Switzerland, 26-27 Sep. 2002: Proceedings, CERN Yellow Report 2004-011.
- [8] Yu.M. Andreiev and E.V. Bugaev, Phys. Rev. D **55** (1997) 1233.
- [9] M. Vanderhaeghen, J.M. Friedrich, D. Lhuillier *et al.*, Phys. Rev. C **62** (2000) 025501.
- [10] E.A. Kuraev, N.P. Merenkov and V.S. Fadin, Sov. J. Nucl. Phys. **45** (1987) 486.
- [11] A. Andonov, A. Arbuzov, D. Bardin *et al.*, Comput. Phys. Commun. **174** (2006) 481 [Erratum-ibid. **177** (2007) 623]; <http://sanc.jinr.ru>, <http://pcphysanc.cern.ch>.
- [12] D. Bardin, S. Bondarenko, L. Kalinovskaya *et al.*, *SANCnews: Sector $f f b b$* , Comput. Phys. Commun. doi:10.1016/j.cpc.2007.06.006 [arXiv:hep-ph/0506120].
- [13] G.P. Lepage, J. Comput. Phys. **27** (1978) 192.
- [14] A.A. Akhundov, D.Y. Bardin, G. Mitselmakher and A.G. Olszewski, Sov. J. Nucl. Phys. **42** (1985) 426 [Yad. Fiz. **42** (1985) 671].